Geophysical Turbulence and the Duality of the Energy Flow Across Scales

A. Pouquet[1,2] and R. Marino[2]

[1]*Laboratory for Atmospheric and Space Physics, and Department of Applied Mathematics, University of Colorado, Boulder, Colorado 80309, USA*

[2]*Computational and Information Systems Laboratory, NCAR, Boulder, Colorado 80307, USA*

(Received 10 September 2013; published 3 December 2013)

The ocean and the atmosphere, and hence the climate, are governed at large scale by interactions between pressure gradient and Coriolis and buoyancy forces. This leads to a quasigeostrophic balance in which, in a two-dimensional-like fashion, the energy injected by solar radiation, winds, or tides goes to large scales in what is known as an inverse cascade. Yet, except for Ekman friction, energy dissipation and turbulent mixing occur at a small scale implying the formation of such scales associated with breaking of geostrophic dynamics through wave-eddy interactions or frontogenesis, in opposition to the inverse cascade. Can it be both at the same time? We exemplify here this dual behavior of energy with the help of three-dimensional direct numerical simulations of rotating stratified Boussinesq turbulence. We show that efficient small-scale mixing and large-scale coherence develop simultaneously in such geophysical and astrophysical flows, both with constant flux as required by theoretical arguments, thereby clearly resolving the aforementioned contradiction.

DOI: 10.1103/PhysRevLett.111.234501 PACS numbers: 47.27.ek, 47.32.Ef, 47.55.Hd

Geostrophic balance, in which nonlinearities are neglected, leads to simplified quasibidimensional behavior with energy flowing to large scales, and reduced small-scale dissipation, contrary to observations [1–5]: vertical mixing can decrease water density, contributing to the (upward) closing of the ocean global circulation [1]. It is identified with breaking of internal gravity waves [6], and it can potentially control the amplitude of the mesoscales.

Such flows are neither 3D nor 2D, since at small scales 3D eddies may prevail. Considering the system dimensionality D_S proved essential when examining critical phenomena which simplify in higher dimensions, due to more mode interactions as D_S grows. Fluid turbulence is vastly different in two or three dimensions, because of the strong constraint imposed by the new 2D invariants (such as the integrated powers of vorticity). This leads to energy flowing towards the largest scales, ending up in a condensate [7]; it can take the form of features such as jets, observed in the atmosphere of planets, or in the oceans as striations [8]. Thus, geophysical turbulence is anisotropic, quasi-2D at large scale and quasi-3D at small scale [9].

However, traditional three-dimensional homogeneous isotropic turbulence is known to break structures (mesoscale eddies, clouds) into progressively smaller entities which will be dissipated at small scale, enhancing mixing of tracers such as pollutants [10] or biota [11]. Whereas the fate of energy in 3D is modeled through an enhanced viscosity $\nu_{\rm turb} > 0$, the 2D evolution leading to large-scale structures can be related to a destabilizing transport coefficient, e.g., $\nu_{\rm turb} \leq 0$. Since the direction of the cascade is known to affect the amount of energy available to irreversible processes of dissipation and mixing, it is thus an essential parameter in the overall energy budget of the atmosphere and ocean [12].

A transition from 2D to 3D in turbulence has been investigated in various contexts. For example, is there a critical dimension for which $\nu_{\rm turb}$ changes sign, indicative of a change of behavior in the overall flow dynamics? Using two-layer quasigeostrophic models with bottom friction, it was shown recently that when adding, in a somewhat *ad hoc* fashion, a horizontal eddy-viscosity mimicking coupling to smaller scales and thereby presumably changing locally the sign of $\nu_{\rm turb}$, both a direct and inverse energy cascades were obtained [13].

More formally, starting from two-point turbulence closure, space dimensionality appears through incompressibility. The critical dimension that separates 2D from 3D behavior can be computed and is found to be ≈ 2.05 [14] (see also [15]). A simple model which is a local version (in modal space) of the closure equations, derived in [16], describes the energy flux to the small scales and the large scales by introducing an (unsigned) parameter which represents the ratio of inverse to direct flux,

$$R_\Pi = |\epsilon_I/\epsilon_D|;$$

it is found to be a smooth monotonic function of D_S, in a fashion similar to critical phenomena, thus providing a path between 2D and 3D behavior. In order to model the anisotropy of geophysical flows, one can alternatively introduce an anisotropic scale contraction or dilation. This allows us to break the geostrophy constraint by considering explicitly the production of horizontal vorticity by horizontal or vertical eddies; it leads to a fractal dimension of turbulence, close to 2.55 for stratified flows [17].

Furthermore, an inverse energy cascade can also occur in 3D homogeneous isotropic turbulence. On the one hand, when restricting nonlinear interactions in 3D to those

between helical waves of the same polarization, energy is found to flow to a large scale, with helicity (velocity-vorticity correlations) populating the small scales [18]. In reality, cross-polarization interactions dominate, but the tendency for strong inverse transfer is clearly displayed in this restricted model.

On the other hand, taking a purely 2D input of energy and a fluid with a variable aspect ratio A_r, energy again has an increased tendency to flow to large scales as A_r becomes small, with a transition at $A_r \approx 1/2$ (A_r is defined as the ratio of the vertical resolution to the forcing scale) [19]. A clear dual energy cascade is obtained, with the ratio of inverse to forward flux R_Π being a decreasing function of A_r. Also, inverse transfer in thick layers (now with $A_r \approx 0.78$) is observed experimentally, the suppression of vertical motions being attributed to interactions with vertical shear for eddies whose time scale is larger than the characteristic shear time [20].

These are idealized physical systems, modeling complex fluids under rather restrictive conditions. However, the link between large scales and small scales (or nonlocal interactions between Fourier modes) is embodied in coherent structures such as chlorophyl filaments [21], water vapor, ozone, temperature, or salinity tracer fronts, and in magnetohydrodynamics, current sheets, plasmoids, and Alfvén vortices [22]. These structures have one dimension comparable to the integral scale of the flow or larger and one close to the dissipative scale. One element altering the way such structures arise and evolve is the ideal invariants, and in particular whether or not they involve gradients. Finally, if one expects the symmetries of the primitive equations to recover at small scale, using a statistical argument based on the large number of modes, this recovery may be impeded by the presence of large-scale shear [23]. For example, direct coupling between large scales (at which the inertiogravity waves reside) and small scales (at which turbulence resides) was demonstrated in [24], providing a progressive destruction of shear layers together with propagation, over the layer depth, of efficient mixing induced by the turbulence.

Stratified turbulence is not 2D in the traditional sense: it has strong vertical shearing [9,25–29], allowing for the efficient creation of small scales, as well as of large scales in the presence of rotation [30]. What is perhaps not well recognized is that the 3D Boussinesq equations, including rotation and stratification as in the atmosphere and oceans, can produce both large-scale and small-scale energy excitation, *both* with constant flux. Numerous numerical studies suffer from a lack of resolving both the large and the small eddies: because of the inherent cost of such computations, a divide-and-conquer approach has been successfully followed, analyzing either the direct or the inverse cascade, but not convincingly both. Fluxes of energy to large scales and to small scales become comparable for strong rotation [31], as well as in the presence of stratification [32]. However, in all these studies, the smallness of the forcing wave number (≈ 4 or 5) does not allow for a clear conclusion concerning the existence of the inverse cascade itself.

TABLE I. Runs on cubic grids of n_p^3 points, 10 and 15 representing $n_p = 1024$ and 1536. All runs use a random force in the wave number band $k_F \in [10, 11]$. Re, Fr, and Ro are the Reynolds, Froude, and Rossby numbers, with $N/f = \mathrm{Ro}/\mathrm{Fr}$ and $\mathcal{R}_B = \mathrm{ReFr}^2$ the buoyancy Reynolds number. $R_\Pi = \epsilon_I/\epsilon_D$ is the ratio of the inverse to the direct flux of energy in the vicinity of k_F ($1 < k < 9$ for ϵ_I, $11 < k < 20$ for ϵ_D); it is computed on spectra averaged over 10 turnover times $\tau_{NL} = L_F/U_0$, in the range $12 < t/\tau_{NL} < 22$. Finally, α is the best fit for the small-scale kinetic energy spectral index. Note the significant decrease of α with the increasing strength of small-scale turbulent eddies compared to the waves, as measured by $\mathcal{R}_B$, a parameter related to the ratio of the forcing to the Ozmidov and dissipative scales at fixed N/f. All large-scale ($k < k_F$) spectral indices are close to 5/3 (see Fig. 2).

Run	Re	Fr	Ro	N/f	$\mathcal{R}_B$	R_Π	α
10a	5000	0.020	0.08	4	2.0	5.77	−3.99
10b	5000	0.045	0.18	4	10.1	2.70	−2.93
10c	5000	0.060	0.24	4	18.0	1.36	−2.34
10d	4000	0.040	0.08	2	6.4	9.04	−3.99
10e	5000	0.090	0.18	2	40.5	1.62	−2.12
15a	8000	0.100	0.20	2	80.0	1.08	−1.87

Thus, we now provide numerical evidence of the simultaneous generation of large-scale and small-scale flows, both with constant flux, using direct numerical simulations (DNS) of the Boussinesq equations (see Table I).

Methods.—Oceanic turbulence is studied in the idealized context of the incompressible stably stratified rotating Boussinesq primitive equations, with $\mathbf{u}$ the velocity and θ the density (or temperature) fluctuations in units of velocity. Solid-body rotation of strength Ω_0 (with $f = 2\Omega_0$) is imposed in the vertical (z) direction with unit vector $\hat{z}$, as well as antialigned gravity g; an isotropic three-dimensional forcing function $\mathbf{F}$ is imposed as well:

$$\partial_t \mathbf{u} - \nu\Delta\mathbf{u} + N\theta\hat{z} + \mathbf{F} + \nabla p - f\mathbf{u}\times\hat{z} = -\mathbf{u}\cdot\nabla\mathbf{u}, \tag{1}$$

$$\partial_t \theta - \kappa\Delta\theta - Nw = -\mathbf{u}\cdot\nabla\theta, \tag{2}$$

w being the vertical velocity, p the pressure, ν the viscosity, and $\kappa = \nu$ the thermal diffusivity. $\nabla\cdot\mathbf{u} = 0$ ensures incompressibility. The square Brunt-Väisälä frequency is given by $N^2 = -(g/\theta)(d\bar{\theta}/dz)$, where $d\bar{\theta}/dz$ is the imposed background stratification, assumed to be linear and constant. In the ideal case ($\nu = 0$, $\mathbf{F} = 0$), the total (kinetic plus potential) energy $E_T = \frac{1}{2}\langle|\mathbf{u}|^2 + \theta^2\rangle = E_V + E_P$ is conserved and the pointwise potential vorticity $P_V = -N\omega_z + f\partial_z\theta + \boldsymbol{\omega}\cdot\nabla\theta$ is a material invariant. No modeling of small-scale dynamics is included.

The GHOST code (Geophysical High Order Suite for Turbulence) is pseudospectral and triperiodic, with n_p^3 grid points; it is parallelized with a hybrid MPI/Open-MP method and scales linearly up to 98 000 processors for a grid of up to 6144^3 points [33]. Forcing is introduced in the momentum equation as a random field centered in the wave number band $k_F \in [10, 11]$. The largest resolved scale is adimensionalized to $L_0 = 2\pi$, corresponding to a minimum wave number $k_{\min} = 1$; the smallest resolved scale is $2\pi/k_{\max} = 6\pi/n_p$. Initial conditions are zero for the density fluctuations and random for the velocity.

Three dimensionless parameters characterize the flow: the Reynolds number $\mathrm{Re} = U_0 L_F/\nu$, the Rossby number $\mathrm{Ro} = U_0/[L_F f]$, and the Froude number, $\mathrm{Fr} = U_0/[L_F N]$. $U_0 \approx 1$ is the rms velocity, $L_F = 2\pi/k_F$ is the forcing scale; finally, $\epsilon_V \equiv dE_V/dt = -\langle \mathbf{u} \cdot \mathbf{F} \rangle$ is the kinetic energy injection rate. Note that in order to resolve the Ozmidov scale, $\ell_{\mathrm{oz}} = [\epsilon_V/N^3]^{1/2}$, at which the eddy turnover time and $1/N$ become equal and isotropization recovers, one can show that $\mathcal{R}_B \geq 1$, where $\mathcal{R}_B = \mathrm{ReFr}^2$ is the buoyancy Reynolds number. Runs are performed with $2 < \mathcal{R}_B \leq 80$ (see Table I). Whether the Ozmidov scale is properly resolved or not may well alter the efficiency of mixing, and the properties of stratified turbulence, as advocated in [27] and as also observed here.

The right-hand sides of Eqs. (1) and (2) are used to derive the evolution of the total (kinetic plus potential) energy density. Taking its Fourier transform (denoted by $\hat{\cdot}$, with $\star$ denoting complex conjugate) gives access to the spectral transfer which, upon integration over the wave number, yields the total isotropic energy flux $\Pi_T = \Pi_V + \Pi_P$:

$$\Pi_V(k) = \int_{k_{\min}}^{k} T_V(q) dq,$$
$$T_V(q) = -\sum_{\mathcal{C}_q} \hat{\mathbf{u}}_{\mathbf{q}}^{\star} \cdot (\mathbf{u} \cdot \widehat{\nabla \mathbf{u}})_{\mathbf{q}},$$

with $\mathcal{C}_q$ the shell $q \leq |\mathbf{q}| < q + 1$. An expression for Π_P can be written in a similar fashion. Note that in these Boussinesq runs the eventual change of sign of energy fluxes at a "zero-crossing" wave number is given by k_F since the forcing is added at that scale.

Results.—Figure 1 shows full 2D cuts of vertical velocity in the vertical and horizontal for Run 15a; the forcing is roughly 1/10 of the box and one clearly observes both intense small-scale features where dissipation occurs and organized patches significantly larger than the forcing scale, indicative of the dual flux of energy.

Results concerning scale-to-scale distribution in Fourier space are displayed in Fig. 2 for runs with $N/f = 2$ and 4, with the fluxes $\Pi_T(k)$ (right) being averaged for 10 turnover times after the peak of dissipation $t_p \approx 1.3$, which also marks the onset of the inverse cascade. All runs listed in Table I display a clear inverse energy cascade ($k < k_F$), with a negative flux, and with an approximate $k^{-5/3}$ scaling

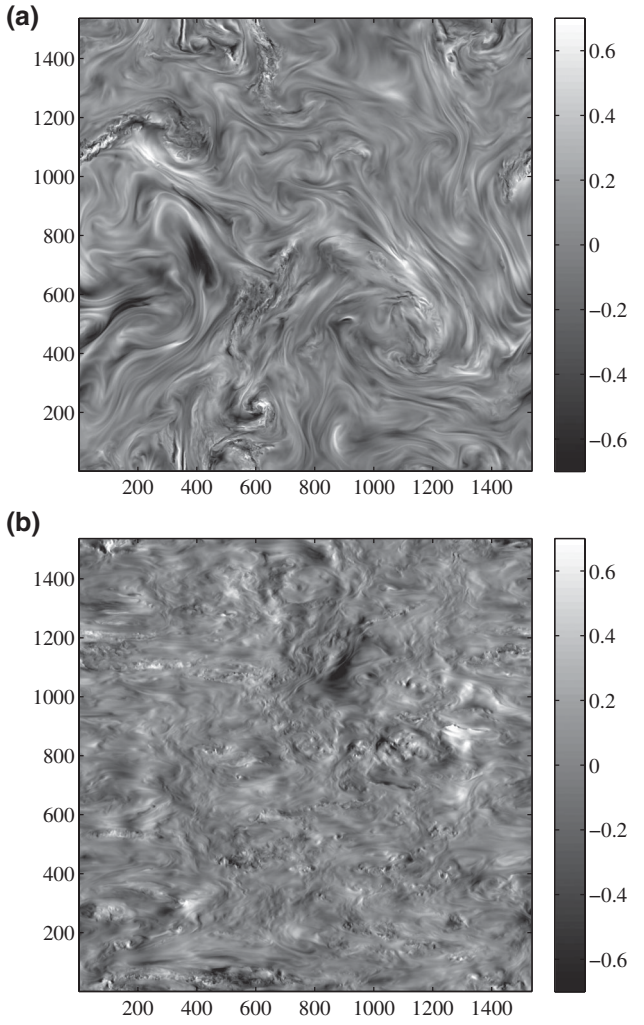

FIG. 1. (a) Horizontal (xy) and (b) vertical (xz) two-dimensional cuts of the vertical velocity for Run 15a at the latest time, with $\mathcal{R}_B \approx 80$ and a small-scale spectrum slightly steeper than a Kolmogorov law. The axes are labeled in terms of grid spacing, and the forcing scale corresponds to roughly 145 in these units. Observe the large-scale structures, with a size of up to a third of the overall flow (or more in the filaments), arising from the inverse cascade, together with superimposed intense small scale eddies (e.g., at $x \approx 200$, $y \approx 1100$ in the top figure). Notice also the different structures in the two cuts, indicative of the persistent anisotropy of the flow.

[30], as expected from classical theory of 2D turbulence [7,34]. This inverse cascade to large scales in 2D was demonstrated using, e.g., two-point closures [35], or more recently, high-resolution DNS [36].

These runs also have a clear direct energy cascade for $k > k_F$, with a constant positive flux. Spectral indices α are defined through $E_V(k) \sim k^{\alpha}$, where the fit is performed in the inertial range of wave number, $k_F < k < k_{\mathrm{diss}}$ with $k_{\mathrm{diss}} \approx k_{\max}$ marking the onset of the dissipation range. These exponents (see Table I) vary between ≈ 3.99 and ≈ 1.87; the steeper, the lower $\mathcal{R}_B$, a parameter that can be

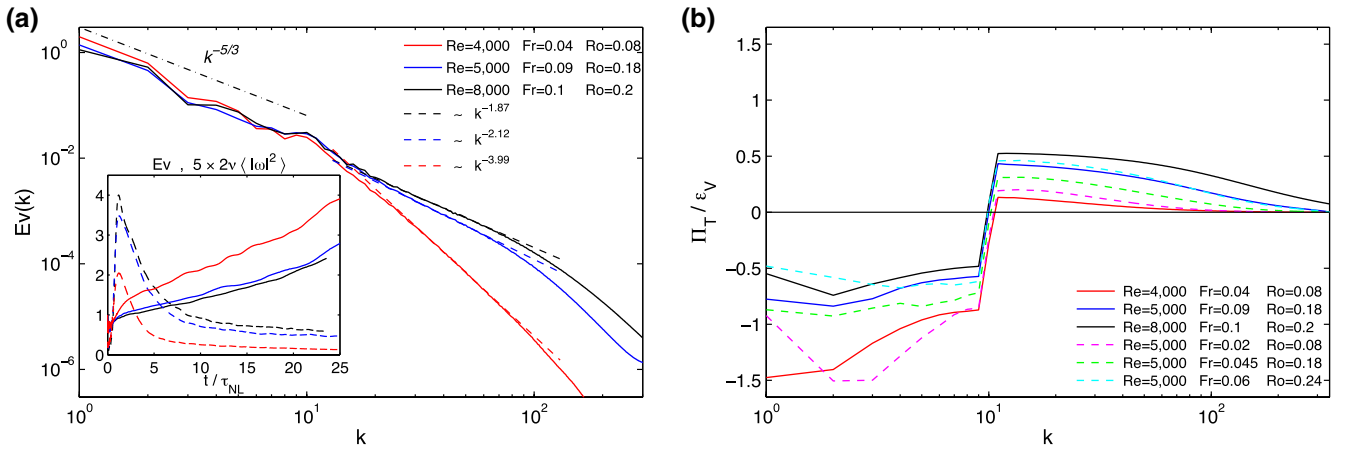

FIG. 2 (color online). (a) Kinetic energy spectra for Run 10d (red line), 10e (blue line), and 15a (black line), all with $N/f = 2$ and increasing $\mathcal{R}_B = \mathrm{ReFr}^2$. The straight lines with different power laws are given as indications. In the bottom inset are shown the temporal evolution of the kinetic energy for the same runs (solid lines), together with their (scaled) dissipation (dashed lines) $5 \times 2\nu\langle|\omega|^2\rangle$, with $\omega = \nabla \times \mathbf{u}$ the vorticity. The spectra, not averaged in time, are shown at $t/\tau_{NL} \sim 22$, whereas the peak of dissipation occurs for all the runs around $t/\tau_{NL} \sim 1.3$, time after which the energy starts to grow, with $\tau_{NL} = L_F/U_0$ the turnover time. (b) Total (kinetic plus potential) energy fluxes normalized by energy input $\epsilon_V = \langle \mathbf{u} \cdot \mathbf{F} \rangle$ for the same runs, as well as for runs 10a (magenta dashed line), 10b (green dashed line), and 10c (cyan dashed line) for which $N/f = 4$.

related to the ratios L_F/ℓ_{oz} and L_F/ℓ_{diss}, where ℓ_{diss} is the dissipation wavelength. The shallower spectrum is close to a Kolmogorov solution $\alpha_{\mathrm{Kol}} = 5/3$, expected (possibly with small intermittency corrections) once the small scales recover isotropy for high enough $\mathcal{R}_B$ (see [31] for the rotating case).

The inset in Fig. 2 gives the temporal variation of E_V (solid lines) and (scaled) dissipation $\mathcal{D}_V = 2\nu\langle|\omega|^2\rangle$ (dashed lines). The steady energy increase, after an initial transient, is typical of inverse cascades. The variation of the ratio of inverse to direct flux with the buoyancy Reynolds number is indicative of the increased effectiveness of turbulence as $\mathcal{R}_B$ grows. One can also expect this ratio to decrease as N/f increases since no inverse cascade occurs in the purely stratified case [30].

Such direct cascades of energy in rotating stratified turbulence have been analyzed using theoretical closure models of turbulence [37]. Dual cascades were also found when examining AVISO altimeter data for the Kuroshio current [13], with values of R_Π approaching those of oceanic data for the largest imposed turbulent (horizontal) viscosity. Whereas these authors conclude to some ambiguity in the interpretation of their results due to the necessary filtering of the data, our DNS of the Boussinesq equations unambiguously show that dual energy cascades are realistic outcomes in a geophysical setting. The higher values of R_Π found in our runs likely reflect the fact that buoyancy is not dominant in our DNS, with $N/f \leq 4$. However, we note that the abyssal southern ocean at mid latitudes has N/f as low as 4 or 5 and shows considerable mixing [1,38].

Conclusion and discussion.—We have shown in this Letter that a dual (direct *and* inverse) constant flux energy cascade is present in rotating stratified turbulence, thereby resolving the paradox noted by some authors (see, e.g., [4,13]) and thus adding credence to having both geostrophic balance and anomalous transport in geophysical turbulence. The computations clearly point out the possibility of the coexistence in the ocean and the atmosphere of idealized large-scale dynamics dominated by quasigeostrophic motions, together with the production of small scales, essential to transport [38].

More computations and data analysis are required to categorize in a quantitative way the duality of the energy cascade, as well as the mixing efficiency one can expect in rotating stratified flows. For example, the variation of R_Π with the relevant dimensionless parameters, such as Re, N/f, and $\mathcal{R}_B$, as well as $L_F = 2\pi/k_F$ (when measured relative to L_0, ℓ_{oz} and ℓ_{diss}), is an open problem which will require huge numerical as well as observational resources. In that context, two-point closures of turbulence (see, e.g., [9]), so-called shell models as used in [16] but generalized to include both rotation and stratification, as well as subgrid scale modeling of small-scale dynamics may be introduced to study this phenomenon in a thorough parametric fashion (see, e.g., [39] for rotating flows), varying the forcing mechanisms as well.

However, there are some indications of a dual flux, using quasigeostrophy [13], or in more complex settings using a numerical oceanic model applied to the California coastal current [40]. This somewhat paradoxical behavior of the energy directivity can be understood if one recalls that triadic energetic exchanges can be either positive or negative, and it is a delicate balance between the two that determines the overall sign of the flux, as also found for helical flows [18].

Physical descriptions beyond the Boussinesq equations can be used in modeling geophysical turbulence. For example, one can consider the evaporatively driven (as opposed to radiatively driven) configurations of stratocumulus clouds, in which case the buoyancy term is altered by the existence of a threshold (in saturation mixture fraction), leading to a nonlinear equation of state. Similar phenomena may occur in the oceans, for which there is a complex set of state relations between temperature, density, and salinity which may lead to distorted isopycnal surfaces. However, using the Boussinesq framework, it is clear that, beyond the energy cascades with small-scale or (exclusive) large-scale constant fluxes, other—mixed—solutions are found that can explain how the oceanic and atmospheric systems are in quasigeostrophic balance at large scale and yet have a sufficient production of small scales leading to enhanced mixing.

We acknowledge B. Galperin and C. Herbert for fruitful discussions. This work is supported by NSF through Grant No. CMG/1025183 and by NCAR. Computations were performed at NCAR (ASD), Grants No. NSF/XSEDE TGPHY-100029 and No. 110044 and Grant No. INCITE/DOE DE-AC05-00OR22725.

[1] J. R. Ledwell, E. T. Montgomery, K. L. Polzin, L. St-Laurent, R. W. Schmitt, and J. M. Toole, Nature (London) **403**, 179 (2000).
[2] J. Vanneste, Annu. Rev. Fluid Mech. **45**, 147 (2013).
[3] B. Hoskins and F. Bretherton, J. Atmos. Sci. **29**, 11 (1972).
[4] M. Molemaker, J. McWilliams, and X. Capet, J. Fluid Mech. **654**, 35 (2010).
[5] G. Ivey, K. Winters, and J. Koseff, Annu. Rev. Fluid Mech. **40**, 169 (2008).
[6] M. Nikurashin, G. K. Vallis, and A. Adcroft, Nat. Geosci. **6**, 48 (2012).
[7] R. Kraichnan and D. Montgomery, Rep. Prog. Phys. **43**, 547 (1980).
[8] B. Galperin, H. Nakano, H.-P. Huang, and S. Sukoriansky, Geophys. Res. Lett. **31**, L13 303 (2004).
[9] P. Sagaut and C. Cambon, *Homogeneous Turbulence Dynamics* (Cambridge University Press, Cambridge, England, 2008).
[10] B. I. Shraiman and E. Siggia, Nature (London) **405**, 639 (2000).
[11] P. Klein and G. Lapeyre, Annu. Rev. Mar. Sci. **1**, 351 (2009).
[12] R. Ferrari and C. Wunsch, Annu. Rev. Fluid Mech. **41**, 253 (2009).
[13] B. Arbic, K. Polzin, R. Scott, J. Richman, and J. Shriver, J. Phys. Oceanogr. **43**, 283 (2013).
[14] U. Frisch, M. Lesieur, and P. Sulem, Phys. Rev. Lett. **37**, 895 (1976).
[15] J. D. Fournier and U. Frisch, Phys. Rev. A **17**, 747 (1978).
[16] T. Bell and M. Nelkin, Phys. Fluids **20**, 345 (1977).
[17] S. Lovejoy and D. Schertzer, *Multifractal Cascades and the Emergence of Atmospheric Dynamics* (Cambridge University Press, Cambridge, England, 2012).
[18] L. Biferale, S. Musacchio, and F. Toschi, Phys. Rev. Lett. **108**, 164501 (2012).
[19] A. Celani, S. Musacchio, and D. Vincenzi, Phys. Rev. Lett. **104**, 184506 (2010).
[20] H. Xia, D. Byrne, G. Falkovich, and M. Shats, Nat. Phys. **7**, 321 (2011).
[21] A. Davis and X.-H. Yan, Geophys. Res. Lett. **31**, L17 304 (2004).
[22] D. Sundkvist, V. Krasnoselskikh, P. Shukla, A. Vaivads, M. André, S. Buchert, and H. Rème, Nature (London) **436**, 825 (2005).
[23] A. Pumir and B. I. Shraiman, Phys. Rev. Lett. **75**, 3114 (1995).
[24] D. C. Fritts, L. Wang, and J. Werne, Geophys. Res. Lett. **36**, 396 (2009).
[25] P. Billant and J.-M. Chomaz, Phys. Fluids **13**, 1645 (2001).
[26] E. Lindborg, J. Fluid Mech. **550**, 207 (2006).
[27] G. Brethouwer, P. Billant, E. Lindborg, and J.-M. Chomaz, J. Fluid Mech. **585**, 343 (2007).
[28] M. Waite and P. K. Smolarkiewicz, J. Fluid Mech. **606**, 239 (2008).
[29] P. Billant, A. Deloncle, J.-M. Chomaz, and P. Otheguy, J. Fluid Mech. **660**, 396 (2010).
[30] R. Marino, P. Mininni, D. Rosenberg, and A. Pouquet, Europhys. Lett. **102**, 44 006 (2013).
[31] P. Mininni, D. Rosenberg, and A. Pouquet, J. Fluid Mech. **699**, 263 (2012).
[32] H. Aluie and S. Kurien, Europhys. Lett. **96**, 44 006 (2011).
[33] P. Mininni, D. Rosenberg, R. Reddy, and A. Pouquet, Parallel Comput. **37**, 316 (2011).
[34] G. Boffetta and R. Ecke, Annu. Rev. Fluid Mech. **44**, 427 (2012).
[35] A. Pouquet, M. Lesieur, J. C. André, and C. Basdevant, J. Fluid Mech. **72**, 305 (1975).
[36] G. Boffetta, J. Fluid Mech. **589**, 253 (2007).
[37] B. Galperin and S. Sukoriansky, Ocean Dyn. **60**, 1319 (2010).
[38] K. J. Heywood, A. N. Garabato, and D. Stevens, Nature (London) **415**, 1011 (2002).
[39] A. Pouquet, J. Baerenzung, P. Mininni, D. Rosenberg, and S. Thalabard, J. Phys. Conf. Ser. **318**, 042015 (2011).
[40] X. Capet, J. McWilliams, M. Molemaker, and A. Shchepetkin, J. Phys. Oceanogr. **38**, 2256 (2008).